Evaluation of Indices for Automatic Active Fire and Burn Scar Detection in Forest Zones Using Satellite Imagery in Chiang Mai, Thailand

Peeloung, C.[1,2] and Charoenpanyanet, A. [2*]
[1]Office of Research Administration, Chiang Mai University, Chiang Mai, Thailand
E-mail: chanudda.peel@gmail.com, ORCID ID: 0009-0004-0263-6763
[2]Department of Geography, Faculty of Social Sciences, Chiang Mai University, Chiang Mai, Thailand
E-mail: arisara.cmu@gmail.com,[*] ORCID ID: 0000-0001-5750-2560
**Corresponding Author*

DOI: https://doi.org/10.52939/ijg.v22i8.5138

Abstract
Wildfire detection and burn scar mapping in the mountainous areas of Northern Thailand remain challenging due to cloud cover, smoke, revisit intervals, and complex terrain, making index and sensor selection critical for reliable fire monitoring. This study aimed to evaluate and compare the performance of three remote sensing indices for classifying Active Fire and Burn Scar areas in Chiang Mai Province, Thailand, and to identify the most appropriate index and satellite platform for each burned area category. The tested indices included the Burned Area Index (BAI) derived from Landsat 8–9 and Sentinel-2 imagery, the Burned Area Index for Sentinel-2 (BAIS2), and the Normalized Burn Ratio Thermal (NBRT) derived from Landsat 8–9 imagery. Reference areas were prepared by visual interpretation of false-color composite images, supported by hotspot data and wildfire suppression coordinates. Optimal index ranges were determined using a statistical thresholding approach, and classification accuracy was assessed using error matrices. NBRT from Landsat 8–9 performed best for active fire detection, with an optimal range of -0.289–0.260, a thematic coverage of 70.54%, and an Overall Accuracy of 88.16%. NBRT also classified burn scars effectively, with an optimal range of 0.326–0.543, a thematic coverage of 77.14%, and an Overall Accuracy of 91.84%. The Sentinel-2 reflectance-based indices did not provide reliable active fire classification under the applied thresholding approach, possibly because they lack the thermal infrared data needed to capture fire-emitted heat. For burn scar mapping, BAIS2 showed the highest performance, with an optimal range of 0.860–1.031, a thematic coverage of 77.14%, and an Overall Accuracy of 96.58%. These findings demonstrate that an index effective for burn scar mapping is not necessarily suitable for active fire detection, underscoring the need to match index and sensor selection to the intended monitoring objective.

Keywords: Active Fire, Burn Scar, Burn Area Index, Burned Area Index for Sentinel-2, Normalized Burn Ratio, Thermal

1. Introduction

Wildfires are a natural phenomenon in many parts of the world and occur due to both natural processes and human activities. The role of fire differs among ecosystems and regions. Fires caused by lightning are an important natural occurrence of fire in boreal and temperate forest ecosystems [1]. In contrast, many wildfires in tropical regions and Southeast Asia are often associated with human activities such as agricultural burning, land preparation for cultivation, and forest clearing or land-use conversion [2] and [3]. Climate change has led to increasingly severe and prolonged fire-conducive weather conditions, while land-use change and human activities continue to influence fire occurrence patterns in different regions [2] and [4].

This trend is evident in Thailand, where wildfires remain a persistent issue. According to the Department of National Parks, Wildlife and Plant Conservation, the cumulative burned area in Thailand during 1992–2021 was approximately 79,952 km², with most affected areas concentrated in the northern region [5]. A 2024 report by the Geo-Informatics and Space Technology Development Agency (GISTDA), based on VIIRS hotspot data recorded from January to May 2024, identified Chiang Mai, Mae Hong Son, and Tak as the

ISSN: 1686-6576 (Printed) | ISSN 2673-0014 (Online)

provinces with the highest cumulative numbers of hotspots [6]. Approximately 70% of all detected hotspots were located within forested areas, indicating that forests were the primary locations affected by wildfires during the reporting period. Hotspot data have been widely used as supporting information for spatial wildfire monitoring. VIIRS hotspots represent locations where satellite sensors detect thermal anomalies and provide valuable information for near-real-time fire monitoring. However, detection capability depends on several factors, including the spatial resolution of the sensor, fire size, cloud cover, smoke conditions, and satellite overpass timing [7] and [8]. These limitations, VIIRS hotspot data remain an important supporting dataset for wildfire monitoring and spatial wildfire management.

Satellite-based wildfire monitoring plays an important role in burned area mapping, active fire detection, and post-fire impact assessment, particularly in large and inaccessible areas. Satellite image-derived indices have been widely used for monitoring burned areas and assessing burn severity such as Burned Area Index (BAI) [9], Burned Area Index for Sentinel-2 (BAIS2) [10], differenced Normalized Burn Ratio (dNBR) [11] and Normalized Burn Ratio Thermal (NBRT) [12]. During 2020–2026, several studies were conducted to evaluate and compare spectral Indices for burned area mapping, active fire detection, and burn severity assessment by using Sentinel-2 and Landsat in many contexts [13] [14] [15] and [16]. For instance, Sentinel-2 imagery and NBR-based GIS analysis have been used to support burned area detection and mapping at the study-area scale [17].

However, many studies continue to use dNBR, which is calculated from the difference in NBR values between pre-fire and post-fire images [18] [19] and [20]. Although this approach is effective for burn severity assessment, it requires cloud-free imagery acquired both before and after fire occurrence, as well as appropriate image acquisition timing. In practice, such data may not be available for all periods. While the combined use of Landsat 8 and Landsat 9 reduces the Landsat revisit interval to approximately 8 days, and Sentinel-2 provides a revisit interval of approximately 5 days [21] and [22], image availability remains dependent on satellite acquisition paths, cloud conditions, and the timing of fire occurrence in each area. Image differencing approaches based on two acquisition dates may have limitations for timely wildfire detection in many regions.

In response to these limitations, studies conducted in recent years have developed approaches for burned area analysis using more diverse and technical indices and techniques. These include the use of Sentinel-2-derived indices combined with thresholding approach for mapping burned area [23], the assessment of post-fire damage and vegetation recovery using spectral indices and machine learning techniques [24] and [25], the integration of Sentinel-2 and Landsat data for regional wildfire mapping [26], as well as the comparison of indices and machine learning methods for burned area classification [27] [28] and [29]. Nonetheless, direct Active Fire detection using Sentinel-2 data normally requires specialized classification methods, such as active-fire detection frameworks or deep learning approaches, rather than the direct application of conventional burned area indices [30]. Consequently, studies evaluating and comparing the performance of BAI, BAIS2, and NBRT for the classification of Active Fire and Burn Scar from single-date imagery in mountainous tropical forest environments remain limited, especially for studies that systematically compare all three indices under separate Active Fire and Burn Scar classification frameworks in the context of northern Thailand.

The selection of BAI, BAIS2, and NBRT in this study was based on different comparative rationales. BAI is a widely used index for burned area classification based on the red and near-infrared (NIR) bands [9]. In contrast, BAIS2 is an index developed specifically for Sentinel-2, utilizing the red-edge, NIR, and shortwave infrared (SWIR) bands, which are sensitive to changes in vegetation and surface conditions following fire [10]. NBRT, on the other hand, was developed as an extension of NBR by incorporating thermal infrared data into the calculation [12]. This index was applied only to Landsat 8–9 imagery because it requires a thermal infrared band, which Sentinel-2 does not provide. Therefore, it is suitable for evaluating the contribution of thermal data to the classification of Active Fire. The comparison of these three indices provides an opportunity to evaluate the differences between reflectance-based indices and an index incorporating thermal data for the classification of Active Fire and Burn Scar. Accordingly, this study aims to evaluate the performance of BAI, BAIS2, and NBRT derived from Sentinel-2 and Landsat 8–9 satellite data for the classification of two burned area classes, namely Active Fire and Burn Scar, using single-date imagery in the mountainous tropical forest areas of Chiang Mai Province, Thailand.

The study also seeks to determine the optimal index ranges for application within the study area. A key feature of this study is the direct classification of Active Fire and Burn Scar from single-date imagery without the need for pre-fire imagery. The study compares indices derived from different spectral regions and sensor characteristics, namely BAI, BAIS2, and NBRT, within the same study area.

2. Methodology

2.1 Study Area

The study was conducted in Chiang Mai Province (Figure 1), located in Northern Thailand. It covers an area of approximately 20,107 km^2, making it the largest province in the north and the second largest province in the country. The province consists of two major topographic zones: Mountainous areas, which account for approximately 80% of the province and are primarily watershed forests, unsuitable for cultivation, and Foothill plains spanning from north to south. The province's total forest area is 15,403.77 km², which constitutes 69.59% of the total provincial area, and 9.39% of Thailand's total forest area. Chiang Mai is home to diverse types of forests including hill evergreen forest, dry evergreen forest, mixed deciduous forest, dry dipterocarp forest, mixed deciduous-coniferous forest, and dry dipterocarp forest. The forest areas comprise natural forests, forest plantations, and regrowth forests. Additionally, agricultural land covers 12.82% (2,936.68 km²) of the area, while residential and other lands cover 17.26% (3,468.75 km²) [31].

2.2 Data Collection

To study applicable indices for detecting active fire and burn scar areas in Chiang Mai, the following data were used:

2.2.1 Hotspot data

Hotspot data for Chiang Mai Province during 2019–2023 were obtained from the Geo-Informatics and Space Technology Development Agency (Public Organization) (GISTDA). The dataset was derived from thermal anomaly detections by the Visible Infrared Imaging Radiometer Suite (VIIRS) sensor at a spatial resolution of 375 m and is used for wildfire monitoring. These data were analyzed together with wildfire suppression coordinates collected in Chiang Mai Province during the same period by the Forest Fire Control and Operations Division, Protected Area Regional Office 16 (Chiang Mai). The suppression coordinates were derived from field-based wildfire suppression operations conducted by field officers and were used to support the identification of wildfire locations. Hotspot data were used only as supporting reference information and not as direct representations of burned areas. This is because hotspots indicate locations where thermal anomalies were detected at the time of satellite image acquisition and may be influenced by fire size, cloud cover, smoke, and satellite overpass timing. Therefore, hotspot data and wildfire suppression coordinates were used as supporting information for the development of the burned area reference database in this study, as shown in Figure 2.

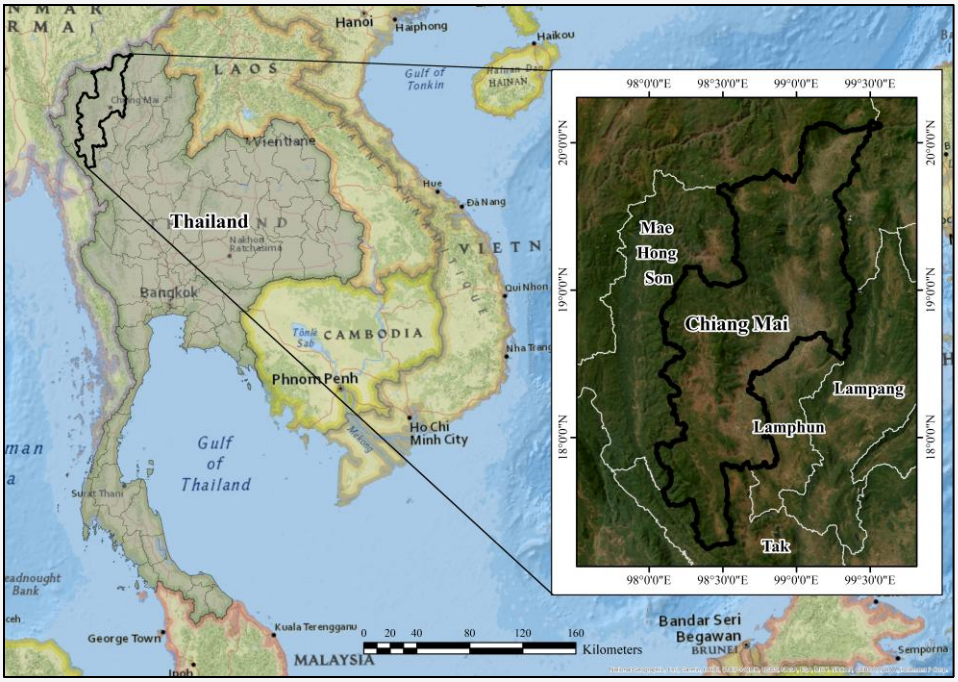

Figure 1: Location of the study area in Chiang Mai Province, northern Thailand

ISSN: 1686-6576 (Printed) | ISSN 2673-0014 (Online) | © Geoinformatics International

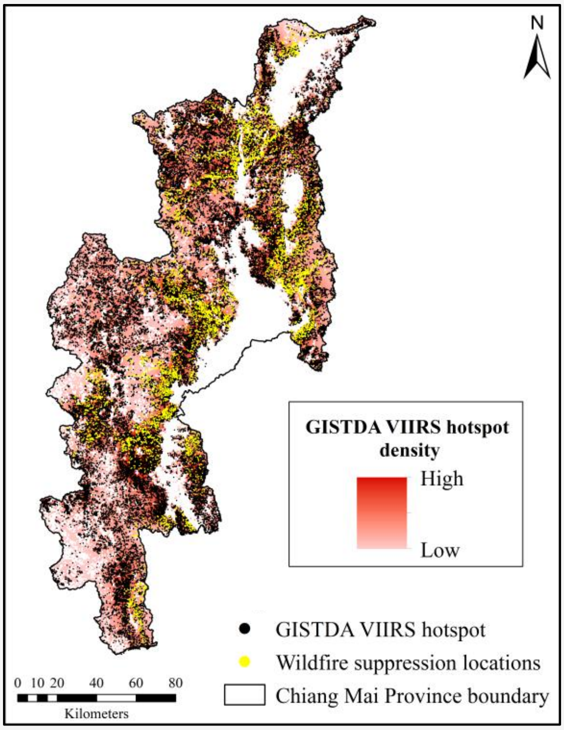

Figure 2: Spatial distribution of GISTDA VIIRS hotspot density and wildfire suppression locations in Chiang Mai Province during January–April 2019–2023

2.2.2 Satellite imagery data

The satellite imagery used in this study consisted of Sentinel-2, Landsat 8, and Landsat 9 data. Surface reflectance products were used because they are suitable for spectral analysis and index calculation. The imagery covered the period from January to April during 2019–2023 (5 years) within the study area of Chiang Mai Province. This period corresponds to the peak wildfire season in Northern Thailand, during which extensive burning and a high number of hotspots are typically observed. For Landsat 8–9, one image per month was used because a single image could cover the entire study area. In contrast, two Sentinel-2 images acquired within a two-day interval during the same monthly observation period were required each month and were mosaicked to achieve complete coverage of Chiang Mai Province, as a single Sentinel-2 image could not fully cover the study area. The satellite imagery used in this study is summarized in Table 1.

2.2.3 Active fire and burn scar reference data

Data on actively burning areas (Active Fire) and burn scar areas (Burn Scar) observed in Sentinel-2, Landsat 8, and Landsat 9 satellite images from January to April, 2019 - 2023, were collected through visual interpretation of false-color composite images. Digitizing was performed to ensure that sample areas were distributed throughout the study area, and that for each month, unique sample areas were selected, thereby creating a spatial reference database for subsequent index threshold determination and classification accuracy assessment. To minimize interpretation bias associated with visual interpretation, all digitization was performed by the same researcher throughout the study period to ensure consistency in image interpretation criteria and delineation of area boundaries. GISTDA hotspot data and wildfire suppression coordinates were used to support verification of the reference areas. Details of the reference data preparation process and consistency verification are provided in Section 2.3.1.

2.3 Methods

2.3.1 Reference database of burned areas

A burned area reference database was developed for forest areas to support index threshold determination and classification accuracy assessment. The database was generated through visual interpretation of satellite imagery together with hotspot data and wildfire suppression coordinates, which were used as spatial reference information for the analysis. The reference data were classified into two classes: Active Fire and Burn Scar. For the development of the reference database, visual interpretation was performed using false-color composite images. Sentinel-2 imagery was displayed using Bands 12 (SWIR2), 8 (NIR), and 4 (Red), while Landsat 8–9 imagery was displayed using Bands 7 (SWIR2), 5 (NIR), and 4 (Red), respectively. The use of SWIR2, NIR, and Red bands enhances the discrimination of burned areas from surrounding land cover. Visual interpretation was based on color characteristics observed in the false-color composite images. Active Fire areas commonly appeared in shades of red, orange, or magenta due to the strong spectral response of actively burning areas in the SWIR region when displayed in the selected band combination. Burn Scar areas generally appeared as dark purple tones, providing clear visual contrast with the surrounding unburned vegetation, which appeared in shades of green. Positional uncertainty may be associated with the hotspot data and wildfire suppression coordinates used to support visual interpretation. In addition, visual interpretation may introduce thematic uncertainty, especially where the spectral signatures of Active Fire and Burn Scar are similar.

ISSN: 1686-6576 (Printed) | ISSN 2673-0014 (Online) | © Geoinformatics International

Table 1: Acquisition dates of Sentinel-2 and Landsat 8-9 images used for active fire and burn scar analysis in Chiang Mai Province, 2019–2023

Year	Month	Satellite	Sensor	Acquisition dates
2019	January	Landsat 8	OLI/TIRS	29 January
	February	Landsat 8	OLI/TIRS	14 February
	February	Sentinel-2	MSI	22 and 24 February
	March	Landsat 8	OLI/TIRS	2 March
	March	Sentinel-2	MSI	9 and 11 March
	April	Landsat 8	OLI/TIRS	3 April
	April	Sentinel-2	MSI	8 and 10 April
2020	January	Landsat 8	OLI/TIRS	16 January
	January	Sentinel-2	MSI	28 and 30 January
	February	Sentinel-2	MSI	12 and 14 February
	February	Landsat 8	OLI/TIRS	17 February
	March	Landsat 8	OLI/TIRS	4 March
	March	Sentinel-2	MSI	28 and 30 March
	April	Sentinel-2	MSI	17 and 19 April
	April	Landsat 8	OLI/TIRS	21 April
2021	January	Landsat 8	OLI/TIRS	2 January
	January	Sentinel-2	MSI	22 and 24 January
	February	Sentinel-2	MSI	1 and 3 February
	February	Landsat 8	OLI/TIRS	3 February
	March	Sentinel-2	MSI	3 and 5 March
	March	Landsat 8	OLI/TIRS	7 March
	April	Sentinel-2	MSI	22 and 24 April
	April	Landsat 8	OLI/TIRS	24 April
2022	January	Sentinel-2	MSI	22 and 24 January
	February	Sentinel-2	MSI	11 and 13 February
	February	Landsat 9	OLI-2/TIRS-2	14 February
	March	Sentinel-2	MSI	3 and 5 March
	March	Landsat 8	OLI/TIRS	26 March
	April	Landsat 8	OLI/TIRS	11 April
	April	Sentinel-2	MSI	12 and 14 April
2023	January	Sentinel-2	MSI	22 and 24 January
	January	Landsat 8	OLI/TIRS	24 January
	February	Sentinel-2	MSI	11 and 13 February
	February	Landsat 8	OLI/TIRS	25 February
	March	Sentinel-2	MSI	28 and 30 March
	March	Landsat 8	OLI/TIRS	29 March
	April	Landsat 9	OLI-2/TIRS-2	6 April
	April	Sentinel-2	MSI	7 and 9 April

To minimize sources of uncertainty, all digitization was performed by the same researcher throughout the entire study period to maintain consistency in interpretation criteria and boundary delineation.

In addition, multiple sources of information were used including the GISTDA hotspot data, wildfire suppression coordinates, and temporal analysis of satellite imagery to examine changes in surface conditions before and after fire occurrence. These datasets were utilized collectively to support classification decisions. Areas affected by clouds, cloud shadows, or smoke were excluded from the reference dataset.

For the development of the reference dataset, imagery acquired during January–April 2019–2023 was used to identify and digitize burned areas, which were subsequently stored as spatial data. A total of 10 sample areas were selected per month, covering both Active Fire and Burn Scar classes. The sample size was determined based on the availability of cloud-free satellite imagery and the number of wildfire events that could be reliably identified during each period. A total of 190 reference samples were collected for each satellite dataset, consisting of 95 Active Fire samples and 95 Burn Scar samples. These samples were spatially and temporally distributed throughout the study period, with unique sample areas selected each month to reduce repeated sampling and spatial–temporal sampling bias. The 190 reference samples were therefore considered appropriate for the objectives of this study, which focused on site-specific index threshold determination and comparative classification accuracy assessment. Although the samples may not fully represent the observed variability of fire-affected areas characteristics across Chiang Mai Province in a statistical sense, they were carefully selected to serve as reference data for index threshold determination and classification accuracy assessment within the scope of this study. Nevertheless, the sample size may not fully represent the variability of burned areas across different forest types, topographic conditions, fire intensities, and atmospheric conditions. Therefore, the results should be interpreted within the context of Chiang Mai Province and the 2019–2023 study period.

In this study, visual interpretation was used solely for the development of reference data for index threshold determination and classification accuracy assessment. The primary burned area classification was performed using satellite-derived indices, enabling a systematic evaluation and comparison of the performance of different indices. This approach also facilitates application to larger areas and multiple time periods more efficiently than visual interpretation alone.

2.3.2 Burned area analysis

Burned area analysis was conducted using Sentinel-2 and Landsat 8–9 surface reflectance imagery, which is suitable for spectral analysis and index calculation. Cloud and cloud shadow masking were performed prior to analysis. Pixels affected by clouds, cloud shadows, and smoke were designated as NoData values and excluded from further analysis. No gap-filling was performed using imagery acquired on other dates in order to avoid temporal inconsistencies that could affect burned area analysis. As a result, actively burning areas or burn scars obscured by cloud cover may not have been detected in some cases. Three spectral indices were subsequently calculated, namely the Burned Area Index (BAI), Burned Area Index for Sentinel-2 (BAIS2), and Normalized Burn Ratio Thermal (NBRT), to evaluate their ability to classify wildfire-affected areas, including Active Fire and Burn Scar.

1) Burned Area Index (*BAI*): An index that uses the reflectance values of the Red visible light waveband and the Near-Infrared (*NIR*) waveband to identify areas affected by fire and was calculated using Equation 1:

$$BAI = \frac{1}{(0.1 - RED)^2 + (0.06 - NIR)^2}$$

Equation 1

Where:
BAI = Burned Area Index
RED = Surface reflectance of the red band
NIR = Surface reflectance of the near infrared band

In general, burned areas exhibit higher reflectance in the Red band and lower reflectance in the Near-Infrared (*NIR*) band compared with unburned vegetation. This is because burning reduces chlorophyll content and alters vegetation structure, resulting in changes to spectral reflectance characteristics. Consequently, the BAI can be used to distinguish wildfire-affected areas from unburned areas [9].

2) The Burned Area Index for Sentinel-2 (*BAIS2*) is a modified version of the Burned Area Index (*BAI*) designed specifically for Sentinel-2 imagery. It utilizes reflectance data from the Red-edge, Red, Near-Infrared (*NIR*), and Shortwave Infrared (*SWIR*) bands to improve sensitivity to changes in vegetation condition and surface moisture. *BAIS2* was calculated using Equation 2:

$$BAIS2 = \left(1 - \sqrt{\frac{RE_{740} \cdot RE_{783} \cdot NIR}{RED}}\right) \cdot \left(\frac{SWIR - NIR}{\sqrt{SWIR + NIR}} + 1\right)$$

Equation 2

ISSN: 1686-6576 (Printed) | ISSN 2673-0014 (Online) | © Geoinformatics International

Where:

$BAIS2$ = Burned Area Index
RED = Surface reflectance of the red band
RE_{740} = Surface reflectance of the red-edge band (Central Wavelength = 740nm)
RE_{783} = Surface reflectance of the red-edge band (Central Wavelength = 783nm)
NIR = Surface reflectance of the near infrared band
$SWIR$ = Surface reflectance of the short-wave infrared band 2

The Red-edge bands are sensitive to changes in chlorophyll content and vegetation canopy condition, while the SWIR bands are sensitive to moisture loss caused by heat and burning. These characteristics improve the discrimination of burned areas from unburned areas [10].

3) Normalized Burn Ratio - Thermal (NBRT) was developed as an extension of the Normalized Burn Ratio (NBR) by incorporating thermal infrared data into the calculation to improve the detection of burned areas. *NBRT* was calculated using Equation 3:

$$NBRT = \frac{NIR - SWIR \cdot (0.001 \cdot Thermal)}{NIR + SWIR \cdot (0.001 \cdot Thermal)}$$

Equation 3

Where:

$NBRT$ = Normalized Burn Ratio - Thermal Index
NIR = Surface reflectance of the near infrared band
$SWIR$ = Surface reflectance of the short-wave infrared band
$Thermal$ = Brightness temperature derived from Landsat 8-9 TIRS Band 10

Prior to NBRT calculation, the thermal band was converted to brightness temperature. The resulting brightness temperature data were then integrated with surface reflectance values from the near-Infrared (NIR) and shortwave Infrared (SWIR) bands to enhance the detection of thermal anomalies associated with actively burning areas. In this study, no additional emissivity correction was applied, and the thermal component was not used to estimate absolute kinetic temperature or land surface temperature. Instead, it was used as a relative thermal indicator for comparative burned area detection, following the concept of thermally enhanced spectral indices [12] and [21].

2.3.3 Determination of optimal index ranges

Following the burned area index analysis described in Section 2.3.2, optimal index ranges were determined for the classification of two burned area classes: Active Fire and Burn Scar. A statistical thresholding approach based on the mean and standard deviation (S.D.) of burned area index values was applied. The reference dataset was divided into two subsets: 70% of the samples were used for index threshold determination, while the remaining 30% were reserved for classification accuracy assessment. To determine the index ranges, the mean and standard deviation of index values were calculated from the 70% subset separately for each burned area class and for each index. The resulting statistics were then used to define the index ranges according to Equation 4.

$$Range = Mean \pm S.D$$

Equation 4

The use of Mean ± 1.0 S.D. as the primary criterion for index threshold determination was based on the application of the mean and standard deviation to describe the distribution of index values within the reference samples. This range constrains the classification threshold to values close to the central tendency of the data and reduces the risk of selecting overly broad thresholds that may result in non-target areas being classified as burned areas. The approach was used to establish preliminary threshold ranges prior to evaluation with the testing dataset and is consistent with previous studies that used mean and standard deviation for burned area threshold determination [32] and [33].

In addition, a sensitivity analysis was conducted using four threshold levels: Mean ± 0.5 S.D., Mean ± ⅔ S.D., Mean ± 1.0 S.D., and Mean ± 1.5 S.D. The threshold ranges derived from each level were evaluated using the remaining 30% of the reference dataset. The evaluation considered both thematic coverage of the reference burned areas and the degree of over-classification in non-burned areas. It should be noted that thematic coverage was used only to assess the proportion of reference areas captured by each threshold range and was not used as the sole criterion for evaluating index performance. Comparative results for the tested threshold levels are presented in Section 3. Based on the comparison, Mean ± 1.0 S.D. was selected because it provided the most balanced trade-off between reference burned area coverage and the reduction of over-classification compared with the other threshold levels tested.

2.3.4 Accuracy assessment

The burned area classification results derived from the optimal index ranges for each index using Sentinel-2 and Landsat 8–9 imagery were evaluated using an error matrix. Four classification accuracy metrics were considered: (1) Producer's Accuracy (PA), (2) User's Accuracy (UA), (3) Overall Accuracy (OA), and (4) the Kappa statistic (K), following the approach of [34]. The assessment was conducted separately for the two burned area classes, namely Active Fire and Burn Scar, to compare the classification performance of each index. In this study, an OA value greater than 85% was used as a reference criterion for assessing classification quality, consistent with commonly adopted practices in remote sensing classification studies [35]. A Kappa value greater than 0.80 was considered indicative of almost perfect agreement according to the criteria proposed by [36]. However, the interpretation of classification performance was not based solely on OA and Kappa values. Producer's Accuracy and User's Accuracy were also considered to evaluate the classification accuracy of each burned area class. Since Kappa values may be influenced by the distribution of observations within the error matrix, the Kappa statistic was reported primarily to facilitate comparison with previous studies in the same field. The workflow of this study is illustrated in Figure 3. The process began with the development of a reference burned area database through visual interpretation of false-color composite satellite imagery, supported by hotspot data and wildfire suppression coordinates. The reference data were then classified into two classes: Active Fire and Burn Scar. Subsequently, the dataset was divided into two subsets, consisting of training data and testing data in a 70:30 ratio. The training dataset was used to determine the optimal index ranges for each burned area index, whereas the testing dataset was used to assess classification accuracy and compare the performance of different indices in burned area classification.

3. Results

The results of the study to evaluate applicable indices for detecting active fires and burn scars in Chiang Mai Province can be divided into following three points:

3.1 Burned Area Database Results

For the visualization and interpretation of burned areas, false-color composite imagery was generated using the band combination of SWIR2 (Red), NIR (Green), and Red (Blue) to enhance fire-related characteristics. Active Fire areas in the satellite imagery appeared as bright red to dark pink tones (Figure 4), indicating ongoing combustion and strong SWIR response associated with active combustion.

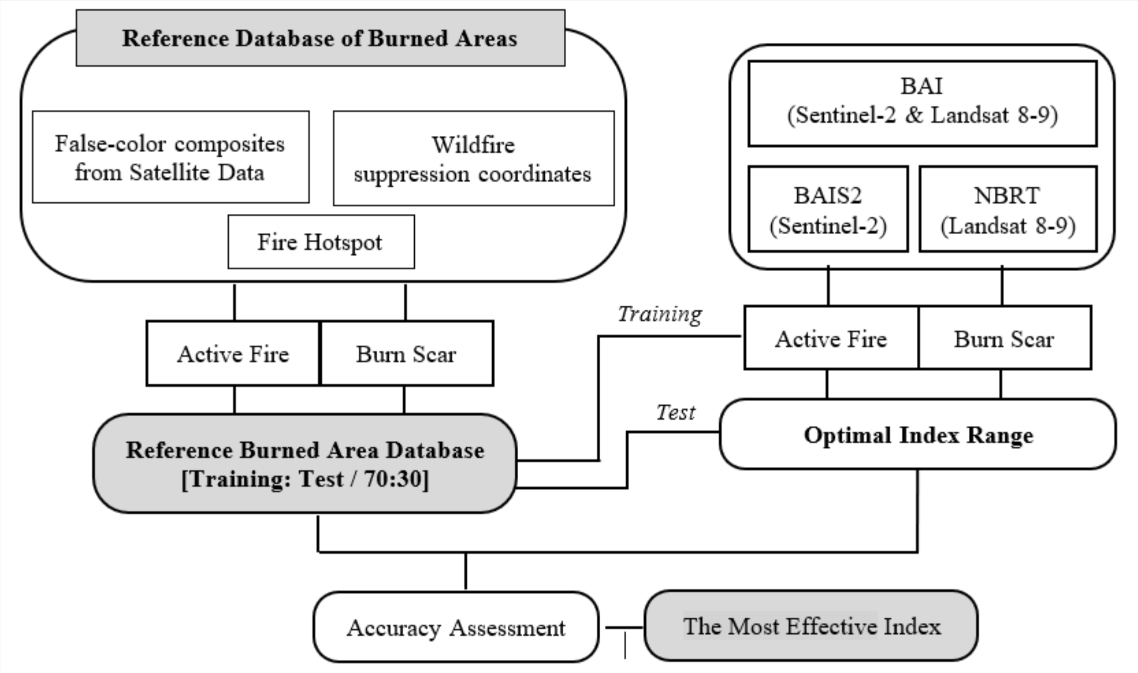

Figure 3: Workflow for reference burned area database construction, training–testing dataset partitioning, optimal index range determination, and classification accuracy assessment

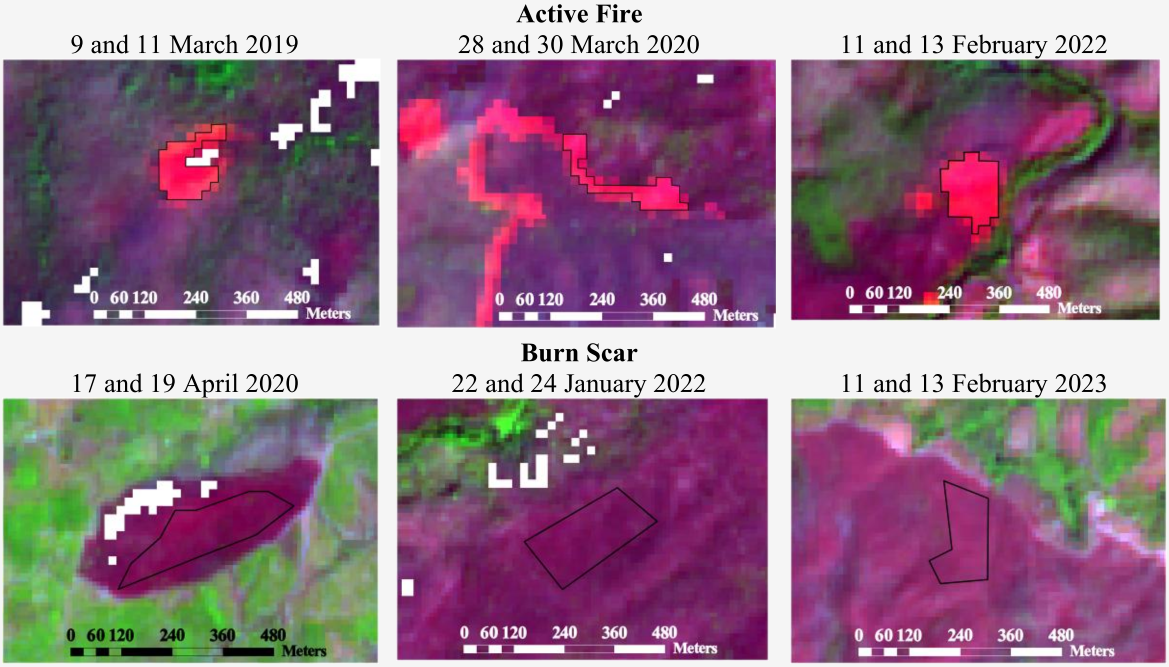

Figure 4: Examples of active fire and burn scar areas from Sentinel-2 imagery using a false-color composite (SWIR2–NIR–Red; Bands 12–8–4). White pixels indicate areas affected by clouds, cloud shadows, or smoke, and black outlines show reference burned area polygons

In contrast, Burn Scar areas appeared as dark purple tones (Figure 5), reflecting vegetation with reduced moisture content and the presence of residual ash following fire events. Pixels displayed in white represent masked areas that were assigned as NoData values due to the effects of clouds, cloud shadows, or smoke, as described in the data preparation procedures (Section 2.3.2). These areas were excluded from the development of the burned area reference database.

A total of 380 burned area reference samples were identified within forest areas (Table 2), consisting of 95 Active Fire samples and 95 Burn Scar samples from each satellite dataset. The results indicate that Burn Scar areas were substantially larger than Active Fire areas. This suggests that most satellite images were acquired after fire events had ceased, allowing burn scars from previous fire events to be identified more frequently than actively burning areas at the time of image acquisition. This pattern is consistent with the nature of wildfires, where the duration of active burning is generally shorter than the satellite revisit interval, thereby limiting the opportunity to capture fires while they are actively burning. A comparison between the two satellite platforms showed that Landsat 8–9 resulted in larger mapped burned area extents than Sentinel-2. This difference may be partly attributed to the coarser spatial resolution of Landsat 8–9, which increases the likelihood of mixed pixels and may result in burn scar areas being represented as larger and more aggregated patches compared with Sentinel-2 imagery, which has a finer spatial resolution. In addition, differences in image acquisition timing between the two satellite systems may also influence their ability to identify burn scars.

3.2 Optimal Index Ranges for Burned Area Classification

The analysis of burned area classification using the three indices, namely the Burned Area Index (BAI) derived from Sentinel-2 and Landsat 8–9 imagery, the Burned Area Index for Sentinel-2 (BAIS2) derived from Sentinel-2 imagery, and the Normalized Burn Ratio Thermal (NBRT) derived from Landsat 8–9 imagery, indicated that the index ranges derived using Mean ± 1.0 S.D. were the most suitable for burned area classification in this study. This finding is consistent with the procedure described in Section 2.3.3, in which four threshold levels (Mean ± 0.5 S.D., Mean ± 0.67 S.D., Mean ± 1.0 S.D., and Mean ± 1.5 S.D.) were evaluated to determine the most appropriate threshold range. The comparative results of the tested threshold levels are presented in Tables 3 and 4.

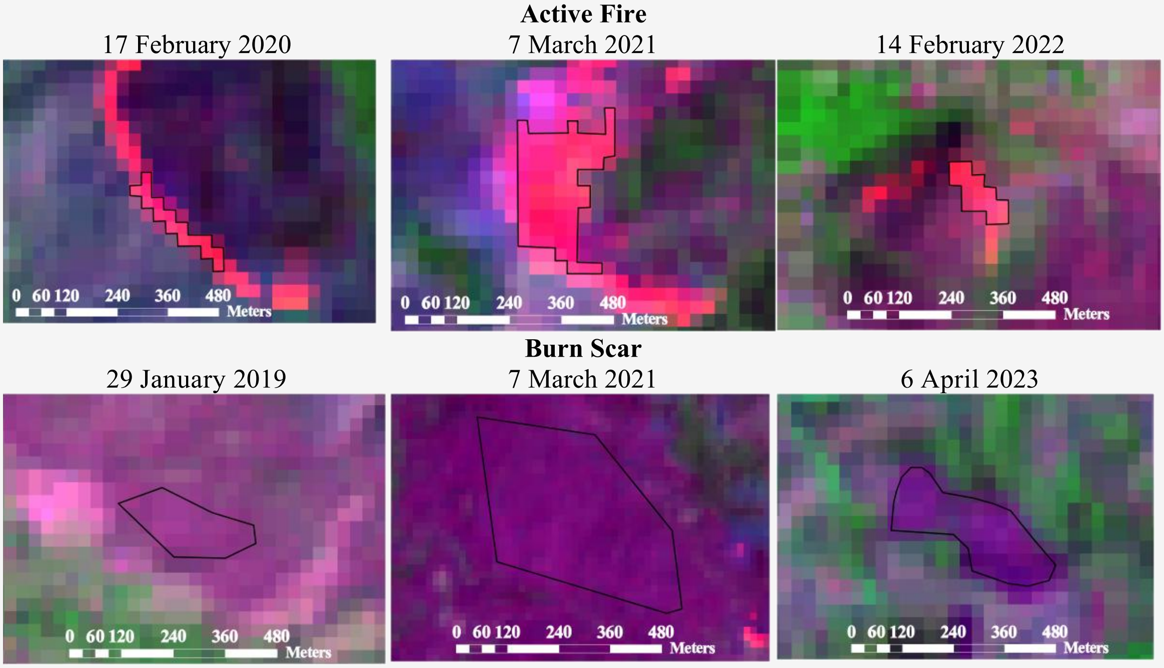

Figure 5: Examples of active fire and burn scar areas from Landsat 8-9 imagery using a false-color composite (SWIR2–NIR–Red; Bands 7–5–4). White pixels indicate areas affected by clouds, cloud shadows, or smoke, and black outlines show reference burned area polygons

Table 2: Reference burned area database by satellite and burned area class used for index range determination and accuracy assessment

	Sentinel-2		Landsat 8-9	
Burned Area	**Area Count**	**Area (km²)**	**Area Count**	**Area (km²)**
Active Fire	95	0.94	95	1.29
Burn Scar	95	2.27	95	6.27
Total	190	3.27	190	7.56

Table 3: Optimal index ranges for each index from Sentinel-2 imagery

	Burned Area Index for Sentinel-2 (BAIS2)				Burn Area Index (BAI)			
	Active Fire		Burn Scar		Active Fire		Burn Scar	
Sentinel-2	**Optimal Range**	**Thematic Coverage (%)**	**Optimal Range**	**Thematic Coverage (%)**	**Optimal Range**	**Thematic Coverage (%)**	**Optimal Range**	**Thematic Coverage (%)**
½ S.D.	1.044 to 1.312	43.57	0.903 to 0.988	42.73	38.335 to 159.933	44.02	124.997 to 233.593	43.93
⅔ S.D.	0.999 to 1.357	55.09	0.889 to 1.002	54.70	18.069 to 180.199	70.20	106.898 to 251.692	55.12
S.D.	0.910 to 1.446	74.20	0.860 to 1.031	76.18	-22.463 to 220.732	88.93	70.699 to 287.891	67.94
1.5 S.D.	0.776 to 1.581	90.96	0.818 to 1.073	88.92	-83.262 to 281.531	91.96	16.401 to 342.189	93.57

Analysis of the narrow threshold ranges, namely Mean ± 0.5 S.D. and Mean ± 0.67 S.D., showed thematic coverage values below 60% for several indices, particularly BAIS2 and NBRT (Tables 3 and 4). This indicates that the threshold ranges were too restrictive, resulting in some burned areas having index values outside the defined thresholds and consequently being omitted from the classification. This effect was especially evident for Burn Scar areas, where burn severity and post-fire conditions varied across locations.

Table 4: Optimal index ranges for each index from Landsat 8-9 imagery

Landsat 8-9	Normalized Burn Ratio - Thermal (NBRT)				Burned Area Index (BAI)			
	Active Fire		Burn Scar		Active Fire		Burn Scar	
	Optimal Range	Thematic Coverage (%)	Optimal Range	Thematic Coverage (%)	Optimal Range	Thematic Coverage (%)	Optimal Range	Thematic Coverage (%)
½ S.D.	-0.147 to 0.125	34.50	0.380 to 0.490	39.50	75.773 to 132.029	39.92	140.959 to 211.759	37.73
⅔ S.D.	-0.192 to 0.170	47.09	0.362 to 0.507	51.49	66.397 to 141.405	55.43	129.159 to 223.559	49.25
S.D.	-0.283 to 0.260	70.54	0.326 to 0.543	77.14	47.652 to 160.156	79.07	105.559 to 247.159	69.80
1.5 S.D.	-0.419 to 0.396	93.60	0.271 to 0.598	94.20	19.517 to 188.284	98.26	70.158 to 282.559	90.61

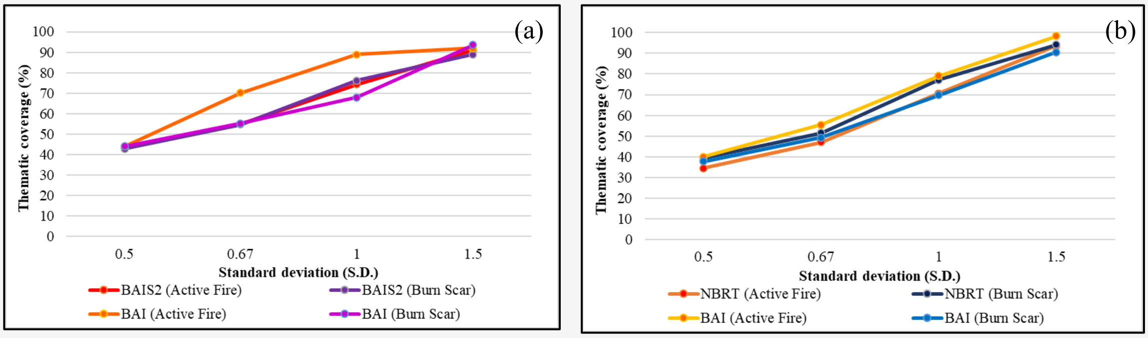

Figure 6: Comparison of burned area thematic coverage (%) at different standard deviation (S.D.) thresholds for burned area indices (a) Sentinel-2, and (b) Landsat 8–9

In contrast, although the Mean ± 1.5 S.D. threshold provided the highest thematic coverage, it produced the widest threshold range among the tested levels, increasing the likelihood of non-burned areas being classified as burned areas and resulting in over-classification. This tendency was particularly apparent for BAI, which showed a greater propensity to classify forested and open areas as burned areas. Therefore, the selection of an appropriate threshold range was not based solely on maximizing thematic coverage, but rather on achieving a balance between burned area coverage and the reduction of over-classification. Based on these considerations, the threshold ranges derived using Mean ± 1.0 S.D. were selected as the most suitable for burned area classification in this study. In this study, thematic coverage refers to the percentage of reference burned areas with index values falling within a specified threshold range. Thematic coverage was used only to evaluate the ability of each threshold range to capture the reference dataset during the threshold determination stage and was not considered a measure of final classification accuracy. The accuracy assessment of the classification results is presented in Section 3.3. As shown in Figure 6, thematic coverage generally increased with higher S.D. values, but at the expense of an increased risk of over-classification. Based on the spatial classification results from the selected examples, BAI derived from Sentinel-2 imagery tended to classify some non-active fire areas, including burn scars and portions of the surrounding landscape, as Active Fire to a greater extent than BAIS2. In contrast, NBRT derived from Landsat 8–9 imagery showed a clearer separation between Active Fire and surrounding areas than BAI, as illustrated in Figure 7. For Burn Scar classification, Figure 8 shows that BAIS2 provided a clearer representation of burn scars and exhibited better agreement with the reference areas than BAI. In the selected example, BAI was unable to effectively identify the burn scar area. Similarly, NBRT derived from Landsat 8–9 imagery showed better agreement with the reference burn scar boundaries than BAI. It should be noted that Figure 7 presents Active Fire examples selected from different locations in Sentinel-2 and Landsat 8–9 imagery because Active Fire is a rapidly changing event and the image acquisition dates of the two satellite systems were not identical. In contrast, Figure 8 presents Burn Scar examples from the same area and from similar acquisition periods to facilitate a clearer comparison of classification results among the indices.

ISSN: 1686-6576 (Printed) | ISSN 2673-0014 (Online) |

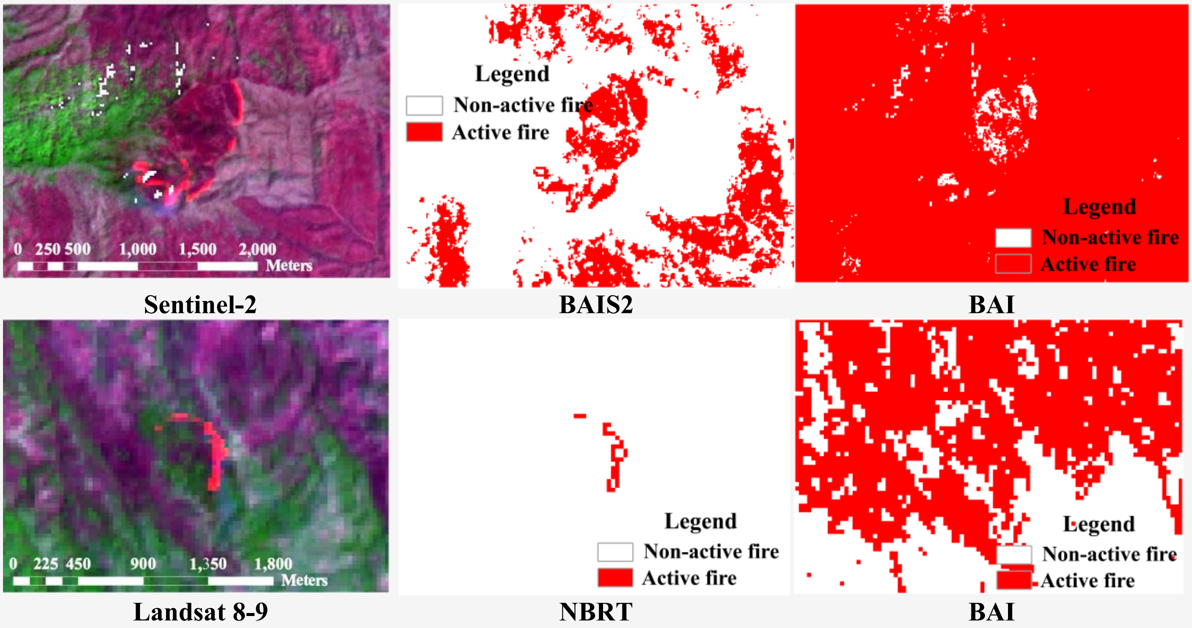

Figure 7: Examples of Active Fire classification results derived from Sentinel-2 and Landsat 8–9 imagery using the optimal index ranges

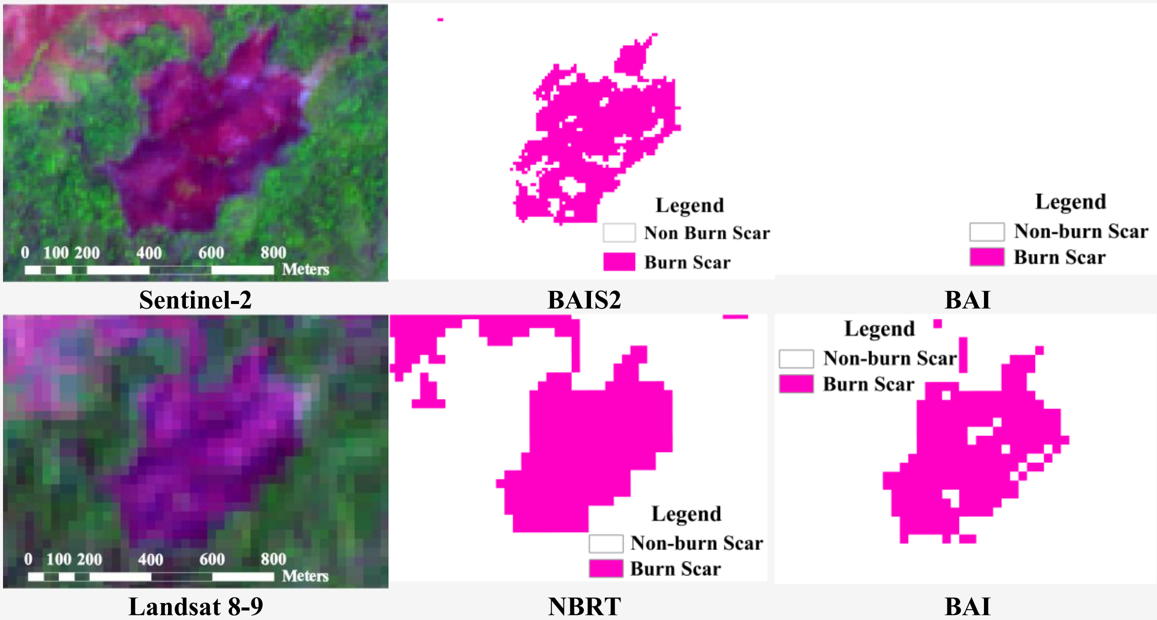

Figure 8: Examples of Burn Scar classification results derived from Sentinel-2 and Landsat 8–9 imagery using the optimal index ranges

After determining the optimal index ranges, sample images with similar acquisition dates were selected to produce example maps of Active Fire classification (Figure 9) and Burn Scar classification (Figure 10) in the forest areas of Chiang Mai Province. From the examination of the sample classification maps in Figures 9 and 10, BAI tended to display larger classified areas than BAIS2 and NBRT in several locations. This is consistent with the over-classification observed from the index threshold evaluation results. These maps help illustrate the spatial distribution patterns of the classification results at the study area scale and support the comparison of spatial classification characteristics among different indices and satellite imagery datasets. In addition to determining optimal index ranges using the mean and standard deviation approach, other threshold determination methods commonly used in remote sensing include ROC analysis and the Otsu method. However, this study selected the Mean ± S.D. approach as a consistent statistical thresholding approach based on the distribution of reference sample values, which allowed multiple indices to be compared using the same reference dataset and selection criteria.

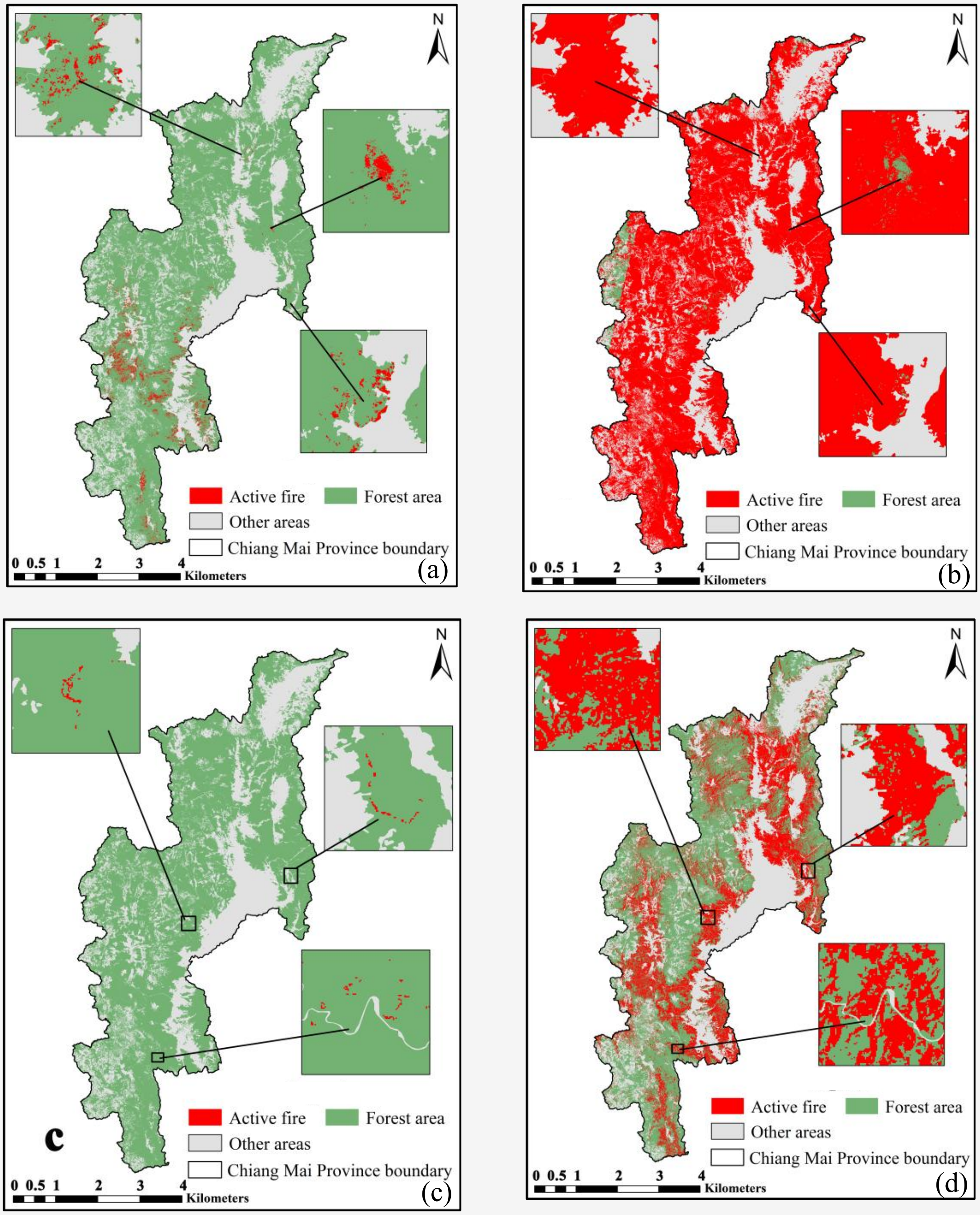

Figure 9: Example maps of Active Fire classification in the forest areas of Chiang Mai Province using the optimal index ranges: (a) Sentinel-2 BAIS2, (b) Sentinel-2 BAI, (c) Landsat 8–9 NBRT, and (d) Landsat 8–9 BAI (3 and 5 March 2021 imagery for Sentinel-2 and 7 March 2021 imagery for Landsat 8–9)

ISSN: 1686-6576 (Printed) | ISSN 2673-0014 (Online) | © Geoinformatics International

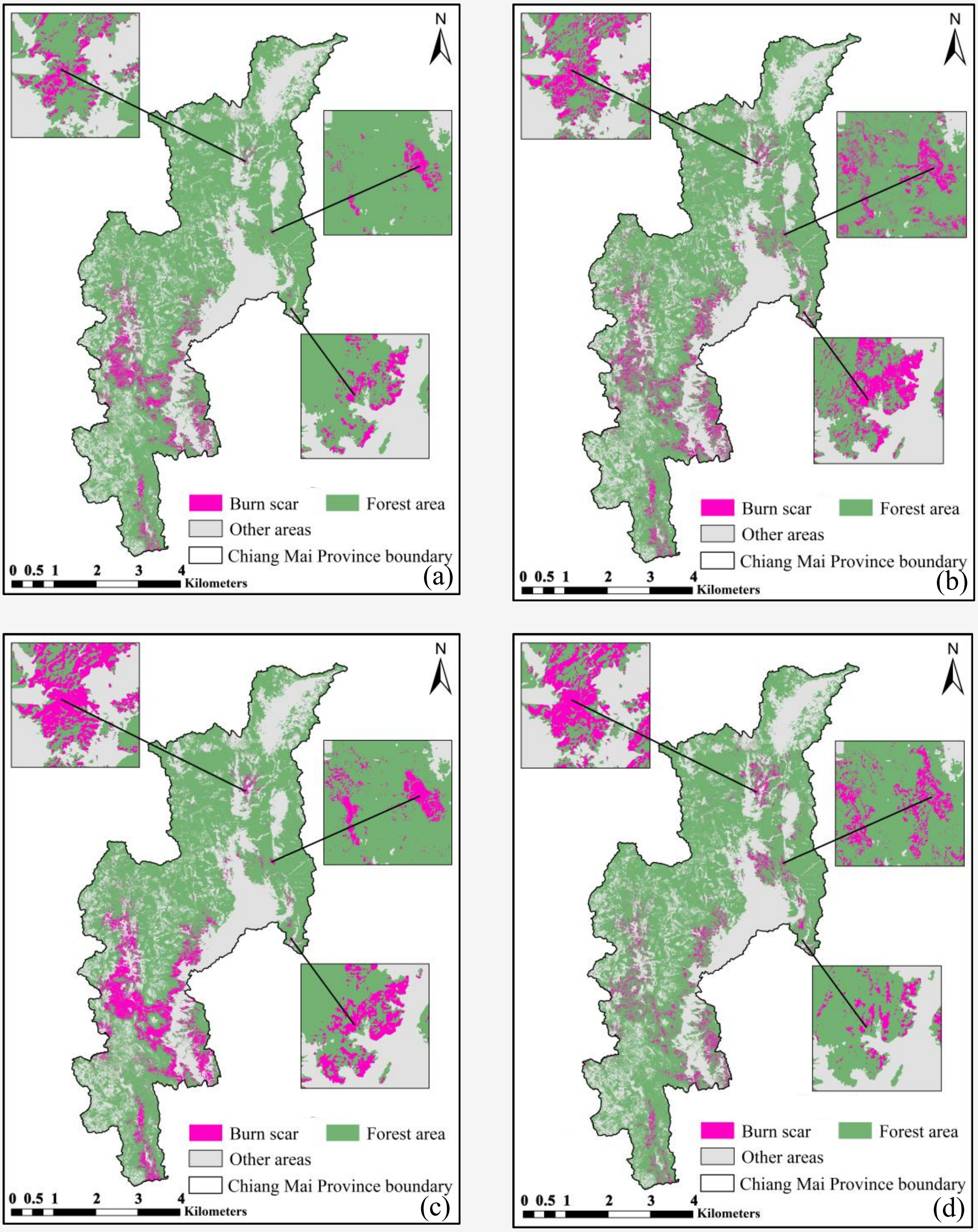

Figure 10: Example maps of Burn Scar classification results in the forest areas of Chiang Mai Province using the optimal index ranges: (a) Sentinel-2 BAIS2, (b) Sentinel-2 BAI, (c) Landsat 8–9 NBRT, and (d) Landsat 8–9 BAI (imagery acquired on 3 and 5 March 2021 for Sentinel-2 and on 7 March 2021 for Landsat 8–9)

3.3 Classification Accuracy Results

The accuracy assessment results of the three indices, namely BAI, BAIS2, and NBRT, derived from Sentinel-2 and Landsat 8–9 imagery, are presented in Table 5. The results demonstrate the performance of each index in classifying Burn Scar and Active Fire areas, which is related to the reflectance data and, where applicable, thermal infrared data used in the calculation of each index.

ISSN: 1686-6576 (Printed) | ISSN 2673-0014 (Online) | © Geoinformatics International

Table 5: Accuracy assessment of burned area classification

BURN INDEX	Burned Area	Accuracy Assessment			
		PA (%)	UA (%)	OA (%)	Kappa
BAIS2	Active Fire	15.26	100.00	57.63	0.15
Sentinel-2	Burn Scar	95.79	97.33	96.58	0.93
BAI	Active Fire	0.00	0.00	49.74	-0.005
Sentinel-2	Burn Scar	75.00	53.16	94.39	0.50
BAI	Active Fire	2.63	83.33	51.05	0.02
Landsat 8-9	Burn Scar	53.16	97.12	75.79	0.51
NBRT	Active Fire	76.32	100.00	88.16	0.77
Landsat 8-9	Burn Scar	85.26	98.18	91.84	0.84

For Burn Scar classification, BAIS2 derived from Sentinel-2 imagery provided the highest classification accuracy among the tested indices. This is because post-fire areas generally exhibit distinct reflectance characteristics in the NIR and SWIR bands, allowing BAIS2 to distinguish burned areas from surrounding areas more effectively than the other indices. In contrast, BAI derived from Sentinel-2 and Landsat 8–9 imagery produced lower Burn Scar classification performance than BAIS2 and NBRT, particularly when considering PA, UA, and Kappa values. Although OA remained high in some cases, BAI was still able to identify burn scars under certain conditions. Since BAI primarily relies on reflectance data from the Red and NIR bands, it may have limitations in distinguishing burned areas from other land cover types with similar spectral characteristics, particularly when compared with indices that incorporate SWIR bands as a major component of the classification process, such as BAIS2 and NBRT. Meanwhile, NBRT derived from Landsat 8–9 imagery performed well across all evaluation metrics and achieved overall classification results comparable to those of BAIS2.

For Active Fire classification, the results indicate that BAI and BAIS2, which rely only on reflectance data, provided low performance in distinguishing actively burning areas. This is because Active Fire areas contain thermal signals generated by combustion, which cannot be directly detected using indices based only on reflectance data. In particular, Sentinel-2 imagery does not contain thermal bands, resulting in lower classification accuracy for Active Fire than for Burn Scar and lower accuracy than NBRT, as shown by the accuracy assessment results in Table 5. Most notably, BAI derived from Sentinel-2 imagery yielded PA and UA values of 0.00% for Active Fire, indicating that this index was unable to detect Active Fire areas within the dataset used in this study. This result suggests that reflectance data alone is insufficient for detecting actively burning areas. In contrast, BAI derived from Landsat 8–9 imagery produced a PA value of 2.63% and a UA value of 83.33%, indicating that although the areas classified as Active Fire were relatively consistent with the reference data, only a small proportion of the actual Active Fire areas was detected. In addition, Active Fire areas are typically small in size and change rapidly over time, making them susceptible to mixed-pixel effects, particularly in moderate-spatial-resolution satellite imagery. Therefore, NBRT derived from Landsat 8–9 imagery provided better Active Fire classification performance than the other indices evaluated in this study when considering PA, UA, OA, and Kappa values together. Since NBRT incorporates thermal data in addition to reflectance data, it is better able to detect actively burning areas than the other indices under the same dataset conditions. Furthermore, NBRT produced Burn Scar classification accuracies comparable to those of BAIS2 and higher than those of BAI according to the values reported in Table 5. These results demonstrate that thermal infrared data substantially improve Active Fire classification because they directly capture thermal signals associated with combustion, whereas Burn Scar classification remains primarily dependent on post-fire changes in spectral reflectance characteristics.

When considering classification accuracy metrics, OA and Kappa showed inconsistent trends in some cases, particularly for the Burn Scar classification results of BAI derived from Sentinel-2 imagery, which produced a high OA value but a moderate Kappa value (K = 0.50, which falls within the moderate agreement range of K = 0.41–0.60 according to the criteria of [36]). This reflects that OA alone may not fully explain classification performance and is consistent with the characteristics of the Kappa paradox, which occurs when the number of samples or pixels in each class of the reference data and classification results is clearly imbalanced. This can cause the Kappa value to appear lower than expected when compared with a high OA value [37] and [38]. Therefore, the interpretation of classification results should consider PA, UA, OA, and Kappa together, as well as the context of the classified data, because these metrics reflect different aspects of classification accuracy, such as the ability to detect reference areas, the reliability of classified areas, overall accuracy, and the level of agreement of the classification results [38] and [39]. When considered together with the classification results in Table 5, the reflectance-based indices, namely BAI and BAIS2, clearly produced lower Active Fire classification performance than the index using thermal data. NBRT derived from Landsat 8–9 imagery provided better Active Fire classification performance than the other indices in this study. For Burn Scar classification, NBRT produced accuracy assessment results comparable to BAIS2 in several metrics and had a higher Kappa value than BAI. In addition, the Kappa value of NBRT for Active Fire was 0.77, which falls within the substantial agreement range (K = 0.61–0.80) according to the criteria of [36]. When considered together with PA, UA, and OA, this indicates that the inclusion of thermal infrared data clearly improves the capability to classify Active Fire, whereas Burn Scar classification remains primarily dependent on post-fire changes in spectral reflectance characteristics. The findings of this study therefore support that thermal infrared data play an important role in Active Fire classification in tropical forest areas.

4. Discussion

The results showed that reflectance-based indices and indices incorporating thermal infrared data produced clearly different performance in classifying Active Fire and Burn Scar areas. The Burned Area Index for Sentinel-2 (BAIS2) derived from Sentinel-2 imagery performed best for Burn Scar classification but had limitations in classifying Active Fire. In contrast, the Normalized Burn Ratio Thermal (NBRT) derived from Landsat 8–9 imagery performed best for Active Fire classification compared with the indices evaluated in this study and also performed well for Burn Scar classification. These results indicate that the selection of a burned area index should be considered according to the type of area to be classified, rather than based solely on threshold values or the percentage of burned area coverage from the reference data. The optimal BAIS2 index range in this study was 0.860–1.446, which is partly consistent with previous findings that BAIS2 values for burned areas are generally higher than 1 [10]. The lower boundary value below 1 in this study may reflect variations in site conditions, burn severity levels, and the characteristics of the reference data used for threshold determination. In addition, this range partially overlaps with the BAIS2 index range of 0.730–1.230 reported by [40] for classifying burn severity levels from Sentinel-2 data. For BAI derived from Landsat 8–9 imagery, the optimal range identified in this study differed from some previous studies [15]. In the case of NBRT, the range identified in this study also differed from a study of burn indices derived from Landsat 8 imagery in Mae Hong Son Province [41]. These differences indicate that thresholds for burned area indices may be sensitive to site context, vegetation type, canopy density, terrain conditions, post-fire surface conditions, and the time elapsed after fire occurrence. Therefore, the determination of site-specific optimal index ranges should be considered carefully, particularly when applying these indices in mountainous forest areas of Thailand.

For Sentinel-2 imagery, BAIS2 gave the best results for Burn Scar classification as compared with BAI. This is because BAIS2 was designed to utilize the spectral characteristics of Sentinel-2 by including the red-edge, near-infrared (NIR), and shortwave infrared (SWIR) bands, which are sensitive to changes in vegetation, moisture, and post-fire surface conditions [10]. In contrast, BAI was designed to classify burned areas using the red and NIR bands and primarily emphasizes the signal of post-fire surfaces [9]. However, although BAIS2 performed well for Burn Scar classification, its Active Fire assessment produced an OA of only 57.63% and a Kappa value of 0.15, indicating that the index range defined for Active Fire was not sufficiently appropriate and that BAIS2 could not classify Active Fire areas effectively when compared with its Burn Scar classification performance. The difference is probably caused by the difference in spectral response between post-fire areas and actively burning areas. Burn Scar areas are due to changes in vegetation, moisture, and surface conditions after fire, which can be reflected relatively clear through the reflectance values in the red edge, NIR, and SWIR bands. The red edge and NIR bands play a role in the differentiation of burned areas based on changes in vegetation and canopy structure, while the SWIR band plays a role in reflecting changes in post-fire surface conditions. Post-fire areas generally show increased reflectance in the SWIR region while reflectance in the NIR region generally decreases [42][43] and [44]. This response therefore mainly reflects the characteristics of post-fire areas and does not necessarily mean that indices using red-edge, NIR, and SWIR bands can always detect actively burning fires effectively. Active Fire is a phenomenon occurring during combustion and is directly associated with thermal energy emitted from fire, rather than post-fire changes in reflectance values [45]. Although Sentinel-2 data in the reflective wavelengths can be used to detect Active Fire in some cases, this generally requires classification methods specifically designed for Active Fire areas rather than the direct use of burned-area indices [46].

When considering the Active Fire assessment results from Sentinel-2 imagery, BAI produced PA and UA values of 0%, whereas BAIS2, although producing a high UA value of 100%, had a PA value of only 15.26% and a Kappa value of 0.15. This reflects that BAIS2 detected only a limited proportion of Active Fire areas, and that the index range used was not sufficiently effective for classifying actively burning areas. These results indicate that many pixels defined as Active Fire in the reference data did not fall within the index range specified for actively burning fire classification. This was particularly evident for BAI, which was unable to classify Active Fire areas from Sentinel-2 imagery. This is because BAI and BAIS2 were designed to emphasize changes in surface reflectance after burning [9] and [10]. When Active Fire occurs only within part of a pixel, the recorded reflectance value becomes a mixed signal from actively burning areas, unburned vegetation, partial burn scars, and surrounding surfaces. In addition, the SWIR values recorded from fire-affected pixels in daytime imagery may be obscured or mixed with solar radiation reflected from surrounding surfaces if the fire does not occupy a sufficiently large proportion of the pixel [45]. Without thermal infrared data to separate thermal energy emitted from fire from such mixed signals, the index values of Active Fire pixels are likely to fall outside the defined threshold range. This results in a very high omission error, leading to PA and UA values of 0% in the case of BAI derived from Sentinel-2 imagery. These results therefore reflect the limitations of indices based solely on reflectance data for Active Fire classification and support that the thermal band is an important component for improving the ability to detect actively burning areas.

On the other hand, NBRT derived from Landsat 8–9 imagery produced clearly better Active Fire classification results than BAI. For Active Fire, NBRT produced an OA of 88.16% and a Kappa value of 0.77, whereas BAI produced an OA of 51.05% and a Kappa value of 0.02. For Burn Scar, NBRT produced an OA of 91.84% and a Kappa value of 0.84, which were higher than those of BAI, which produced an OA of 75.79% and a Kappa value of 0.51. These results are consistent with the burned area classification study of [47], which found that NBRT produced higher accuracy than BAI in the context of Landsat 8 imagery. The findings are also consistent with [48], which reported that NBRT was one of the highly effective indices for burned area classification using Landsat 8 OLI/TIRS imagery. The advantage of NBRT may be related to its development as an extension of NBR by incorporating thermal infrared data into the calculation [11]. The inclusion of thermal infrared data therefore improves the ability of NBRT to respond to actively burning areas when compared with indices based solely on reflectance data.

Differences in sensor type and spatial resolution also play a role in the classification results. Sentinel-2 imagery has a spatial resolution of 10–20 m for the main bands used in the analysis, making it suitable for detecting details of Burn Scar areas at a sub-area level, particularly when considered together with the characteristics of BAIS2, which was designed to utilize the red-edge, NIR, and SWIR bands of Sentinel-2 for burned area mapping [10] and [22]. In contrast, Landsat 8–9 OLI imagery has a spatial resolution of 30 m and includes thermal bands from the TIRS sensor with an original sensor spatial resolution of 100 m, which are resampled to 30 m in the data products used together with the reflective bands [21]. Therefore, the interpretation of NBRT should consider both the advantages of the thermal band and the spatial resolution limitation of the thermal band, particularly in cases where burned areas are small or distributed in patches. Spatial resolution limitations may increase the likelihood of mixed pixels and affect errors in identifying or calculating burned areas [49]. However, Landsat 8–9 imagery includes thermal bands from the TIRS sensor, which Sentinel-2 imagery does not have. This allows NBRT to respond to signals related to the heat of Active Fire areas, even though the Landsat thermal band has a lower spatial resolution than the reflective bands. In terms of its effect on Active Fire classification, atmospheric conditions such as clouds, smoke, or haze may obscure actively burning areas, causing such areas to be assigned as cloud/smoke masks and leading to the omission of Active Fire areas. In addition, in this study, areas affected by clouds, cloud shadows, or smoke were assigned as masked or NoData areas according to the data preparation procedure. This may reduce the area available for classification assessment, particularly in the case of Active Fire areas, which occur over a short period and change rapidly. Therefore, the effects of spatial resolution, sensor type, and atmospheric conditions should be considered together when interpreting burned area index values, rather than relying solely on threshold values or statistical accuracy metrics.

A key strength of this study is the evaluation of burned area index performance by clearly separating

ISSN: 1686-6576 (Printed) | ISSN 2673-0014 (Online) | © Geoinformatics International

Active Fire and Burn Scar areas. This differs from previous studies, which have often evaluated burned areas as a whole or mainly focused on burned area mapping, burn severity assessment, or post-fire impact assessment [48] [50] and [51]. This study therefore helps fill this gap by systematically evaluating the two types of burned areas separately under the same context. This allows the differences in the strengths and limitations of each index to be analyzed between the detection of actively burning fires and post-fire burn scars. The results demonstrate that an index that performs well for post-fire burn scars does not necessarily perform well for actively burning areas. Specifically, BAIS2 is suitable for Burn Scar mapping using Sentinel-2 data because it responds well to changes in vegetation and surface conditions after burning. In contrast, NBRT is more suitable for Active Fire classification because it incorporates thermal infrared data. Therefore, an important contribution of this study is that it highlights the functional limitations of different burned area indices and suggests that index selection should correspond to the objective of wildfire monitoring, whether for detecting actively burning fires or mapping post-fire burn scars. In terms of application, the findings indicate that selecting sensors and indices according to wildfire monitoring objectives can support a two-step workflow. This includes using data from sensors with thermal bands, such as Landsat 8–9 together with NBRT, to support the detection or confirmation of Active Fire locations when suitable satellite imagery is available and using Sentinel-2 together with BAIS2 to map Burn Scar areas after fire events at a higher spatial detail.

However, this study has some limitations that should be considered. These include differences in image acquisition timing between Sentinel-2 and Landsat 8–9 imagery, which may affect the comparison of classification results across sensors, particularly in the case of Active Fire. The results were also affected by clouds, smoke, and masked/NoData areas, which are specific limitations of the dataset used in this study. In addition, some reference data may contain positional and temporal uncertainties, although the combined use of image interpretation, hotspot data, and wildfire suppression coordinates helped increase confidence in the identification of burned areas. These limitations may affect the identification of actively burning pixels and the accuracy assessment of the classification results, particularly for Active Fire, which is a short-duration and rapidly changing phenomenon.

5. Conclusion

This study demonstrates that the performance of burned area indices depends on the spectral characteristics of the indices and the capability of satellite sensors to respond to fire-related signals. A key scientific contribution of this study is that Active Fire and Burn Scar should be considered as distinct classification problems: NBRT derived from Landsat 8–9 imagery outperforms BAI and BAIS2 for Active Fire classification in tropical mountainous forest areas, whereas BAIS2 derived from Sentinel-2 imagery provides superior performance for post-fire Burn Scar mapping.

For Active Fire classification, NBRT derived from Landsat 8–9 imagery provided the highest performance (OA = 88.16%, Kappa = 0.77). This is because NBRT incorporates thermal infrared data from the TIRS sensor in the analysis, which helps directly detect thermal signals generated during combustion. For Burn Scar classification, BAIS2 derived from Sentinel-2 imagery provided the highest performance (OA = 96.58%, Kappa = 0.93), using the red-edge, NIR, and SWIR bands, which are sensitive to changes in post-fire surface conditions. This performance is further supported by Sentinel-2's relatively fine spatial resolution (10 m for the visible/NIR bands and 20 m for the red-edge/SWIR bands). However, because Sentinel-2 does not provide thermal infrared bands, BAIS2 has limited capability for Active Fire classification. These results indicate that, under the conditions of this study, selecting an appropriate index together with a suitable sensor is important for burned area classification in the context of mountainous tropical forest areas in Northern Thailand.

The findings of this study can be applied as preliminary guidance for selecting indices and satellite data for wildfire monitoring. For Active Fire mapping, NBRT derived from Landsat 8–9 data should be used to support Active Fire detection and wildfire response planning. For Burn Scar mapping, BAIS2 derived from Sentinel-2 data should be used to support post-fire area assessment and the identification of targets for restoration. This complementary two-sensor approach can be integrated with existing wildfire monitoring systems to improve the efficiency of fire detection, impact assessment, and prioritization of areas for field operations.

However, this study has limitations related to cloud, cloud shadow, and smoke cover, which may reduce the continuity of detection, particularly for Active Fire, which occurs over a short period. In addition, the optimal index ranges presented in this study are specific to Chiang Mai Province and the period from 2019 to 2023. Therefore, they may not be directly applicable to other areas or time periods. Applying these ranges to areas with different fire regimes, vegetation types, or image acquisition conditions may require recalibration. Future studies should test these index ranges in other areas by comparing the classification results with burned area data from MODIS and VIIRS, as well as considering additional indices such as MIRBI, NDSWIR, and ABAI. Furthermore, the integration of field data, satellite data with higher temporal resolution, and machine learning may help improve the accuracy of burned area classification in mountainous tropical forest contexts.

Acknowledgement

Acknowledgement is extended to the Geo-Informatics and Space Technology Development Agency (Public Organization) for providing hotspot data, and to the Forest Fire Control and Operation Division, Protected Area Regional Office 16 (Chiang Mai), for providing wildfire suppression coordinate data. Support from the CMU Proactive Researcher Program, Chiang Mai University is also gratefully acknowledged.

References

[1] Janssen, T. A. J., Jones, M. W., Finney, D., van der Werf, G. R., van Wees, D., Xu, W. and Veraverbeke, S., (2023). Extratropical Forests Increasingly at Risk Due to Lightning Fires. *Nature Geoscience*, Vol. 16. https://doi.org/10.1038/s41561-023-01322-z.

[2] Bowman, D. M. J. S., Kolden, C. A., Abatzoglou, J. T., Johnston, F. H., van der Werf, G. R. and Flannigan, M., (2020). Vegetation Fires in the Anthropocene. *Nature Reviews Earth & Environment*, Vol. 1. https://doi.org/10.1038/s43017-020-0085-3.

[3] Reddington, C. L., Conibear, L., Robinson, S., Knote, C., Arnold, S. R. and Spracklen, D. V., (2021). Air Pollution from Forest and Vegetation Fires in Southeast Asia Disproportionately Impacts the Poor. *GeoHealth*, Vol. 5(9). https://doi.org/10.1029/2021GH000418.

[4] Jolly, W. M., Cochrane, M. A., Freeborn, P. H., Holden, Z. A., Brown, T. J., Williamson, G. J. and Bowman, D. M. J. S., (2015). Climate-induced Variations in Global Wildfire Danger from 1979 to 2013. *Nature Communications*, Vol. 6. https://doi.org/10.1038/ncomms8537.

[5] Sirirat, N., (2022). The Persistent Wildfire Situation in Thailand. *Geo-Informatics and Space Technology Development Agency (Public Organization)*. [Online]. Available: https://www.gistda.or.th/news_view.php?n_id=5414&lang=TH. [Accessed: May 19, 2025].

[6] Geo-Informatics and Space Technology Development Agency (Public Organization), (2024). *Summary Report on the Wildfire and Haze Situation Using Space Technology and Geo-Informatics in 2024*. Bureau of Geo-Informatics Applications and Services, Geo-Informatics and Space Technology Development Agency (Public Organization), Ministry of Higher Education, Science, Research and Innovation, Thailand. [Online]. Available: https://disaster.gistda.or.th/services/download?type=fire. [Accessed: May 19, 2025].

[7] Schroeder, W., Oliva, P., Giglio, L. and Csiszar, I. A., (2014). The New VIIRS 375 m Active Fire Detection Data Product: Algorithm Description and Initial Assessment. *Remote Sensing of Environment*, Vol. 143. https://doi.org/10.1016/j.rse.2013.12.008.

[8] Coskuner, K. A., (2022). Assessing the Performance of MODIS and VIIRS Active Fire Products in the Monitoring of Wildfires: A Case Study in Turkey. *iForest - Biogeosciences and Forestry*, Vol. 15(2). https://doi.org/10.3832/ifor3754-015.

[9] Chuvieco, E., Martín, M. P. and Palacios, A., (2002). Assessment of different spectral indices in the red-near-infrared spectral domain for burned land discrimination. *International Journal of Remote Sensing*, Vol. 23(23). https://doi.org/10.1080/01431160210153129.

[10] Filipponi, F., (2018). BAIS2: Burned Area Index for Sentinel-2. *Proceedings*, Vol. 2(7). https://doi.org/10.3390/ecrs-2-05177.

[11] Key, C. H. and Benson, N. C., (2006). Landscape Assessment (LA). In: Lutes, D. C., Keane, R. E., Caratti, J. F., Key, C. H., Benson, N. C., Sutherland, S. and Gangi, L. J., *FIREMON: Fire Effects Monitoring and Inventory System*. U.S. Department of Agriculture, Forest Service, Rocky Mountain Research Station, Fort Collins, CO, General Technical Report RMRS-GTR-164-CD, LA-1-55. [Online]. Available: https://research.fs.usda.gov/download/treesearch/24066.pdf. [Accessed: Nov. 30, 2025].

[12] Holden, Z. A., Smith, A. M. S., Morgan, P., Rollins, M. G. and Gessler, P. E., (2005). Evaluation of Novel Thermally Enhanced Spectral Indices for Mapping Fire Perimeters and Comparisons with Fire Atlas Data. *International Journal of Remote Sensing*, Vol. 26(21). https://doi.org/10.1080/01431160500239008.

[13] Alcaras, E., Costantino, D., Guastaferro, F., Parente, C. and Pepe, M., (2022). Normalized Burn Ratio Plus (NBR+): A New Index for Sentinel-2 Imagery. *Remote Sensing*, Vol. 14(7). https://doi.org/10.3390/rs14071727.

[14] Howe, A. A., Parks, S. A., Harvey, B. J., Saberi, S. J., Lutz, J. A. and Yocom, L. L., (2022). Comparing Sentinel-2 and Landsat 8 for Burn Severity Mapping in Western North America. *Remote Sensing*, Vol. 14(20). https://doi.org/10.3390/rs14205249.

[15] Guo, R., Yan, J., Zheng, H. and Wu, B., (2024). Assessment of the Analytic Burned Area Index for Forest Fire Severity Detection Using Sentinel and Landsat Data. *Fire*, Vol. 7(1). https://doi.org/10.3390/fire7010019.

[16] Valdiviezo-Navarro, J. C., Castillo-Santiago, M. Á., Téllez-Quiñones, A. and López-Caloca, A. A., (2026). Performance Evaluation of Burn Area Indices for Effective Fire Detection Using Sentinel-2 Satellite Imagery. *Algorithms*, Vol. 19(2). https://doi.org/10.3390/a19020157.

[17] Mahmood, M. R. and Jumaah, H. J., (2023). NBR Index-Based Fire Detection Using Sentinel-2 Images and GIS: A Case Study in Mosul Park, Iraq. *International Journal of Geoinformatics*, Vol. 19(3). https://doi.org/10.52939/ijg.v19i3.2607.

[18] Llorens, R., Sobrino, J. A., Fernández, C., Fernández-Alonso, J. M. and Vega, J. A., (2021). A Methodology to Estimate Forest Fires Burned Areas and Burn Severity Degrees Using Sentinel-2 data. Application to the October 2017 fires in the Iberian Peninsula. *International Journal of Applied Earth Observation and Geoinformation*, Vol. 95. https://doi.org/10.1016/j.jag.2020.102243.

[19] Demir, S. and Başayiğit, L., (2024). Digital Mapping Burn Severity in Agricultural and Forestry Land over a Half-Decade Using Sentinel Satellite Images on the Google Earth Engine Platform: A Case Study in Isparta Province. *Trees, Forests and People*, Vol. 16. https://doi.org/10.1016/j.tfp.2024.100520.

[20] Lee, S. H., Lee, M. H., Kang, T. H., Cho, H. R., Yun, H. S. and Lee, S. J., (2025). Comparative Analysis of dNBR, dNDVI, SVM Kernels, and ISODATA for Wildfire-Burned Area Mapping Using Sentinel-2 Imagery. *Remote Sensing*, Vol. 17(13). https://doi.org/10.3390/rs17132196.

[21] U.S. Geological Survey, (2022). Landsat 8 and Landsat 9 Data Users Handbooks. *U.S. Geological Survey*. [Online]. Available: https://www.usgs.gov/landsat-missions/landsat-project-documents. [Accessed: May 19, 2026].

[22] European Space Agency, (2024). Sentinel-2 Mission. *SentiWiki*. [Online]. Available: https://sentiwiki.copernicus.eu/web/s2-mission [Accessed: May 19, 2026].

[23] Deshpande, M. V., Pillai, D. and Jain, M., (2022). Agricultural Burned Area Detection Using an Integrated Approach Utilizing Multi Spectral Instrument Based Fire and Vegetation Indices from Sentinel-2 satellite. *MethodsX*, Vol. 9. https://doi.org/10.1016/j.mex.2022.101741.

[24] Liu, C. L., Wang, Y. R. and Liu, W. Y., (2025). Multi-index remote sensing for post-fire damage assessment: accuracy, carbon loss, and conservation implications. *Frontiers in Forests and Global Change*, Vol. 8. https://doi.org/10.3389/ffgc.2025.1577612.

[25] Anees, S. A., Mehmood, K., Luo, M., Abuelgasim, A., Pan, S., Shahzad, F., Muhammad, S. and Khan, W. R., (2025). Advancing forest fire burn severity and vegetation recovery assessments using remote sensing and machine learning approaches. *Ecological Informatics*, Vol. 92. https://doi.org/10.1016/j.ecoinf.2025.103446.

[26] Chen, Y., Kou, W., Yin, X., Wang, R., Ye, J. and Wang, Q., (2025). Regional Forest Wildfire Mapping Through Integration of Sentinel-2 and Landsat 8 Data in Google Earth Engine with Semi-Automatic Training Sample Generation. *Remote Sensing*, Vol. 17(24). https://doi.org/10.3390/rs17244038.

[27] Zikiou, N., Rushmeier, H., Capel, M. I., Kandakji, T., Rios, N. and Lahdir, M., (2024). Remote Sensing and Machine Learning for Accurate Fire Severity Mapping in Northern Algeria. *Remote Sensing*, Vol. 16(9). https://doi.org/10.3390/rs16091517.

[28] Chen, X., Zhang, Y., Wang, S., Zhao, Z., Liu, C. and Wen, J., (2024). Comparative Study of Machine Learning Methods for Mapping Forest Fire Areas Using Sentinel-1B and 2A Imagery. *Frontiers in Remote Sensing*, Vol. 5. https://doi.org/10.3389/frsen.2024.1446641.

[29] Roodsarabi, Z., Farhadi, H. and Kiani, A., (2025). Machine Learning-Based Burned Area Detection using Sentinel-2 Imagery and Spectral Indices. *Environmental Monitoring and Assessment*, Vol. 197. https://doi.org/10.1007/s10661-025-14332-8

[30] Zhang, Q., Ge, L., Zhang, R., Metternicht, G. I., Liu, C. and Du, Z., (2021). Towards a Deep-Learning-Based Framework of Sentinel-2 Imagery for Automated Active Fire Detection.

Remote Sensing, Vol. 13(23). https://doi.org/10.3390/rs13234790.

[31] Chiang Mai Provincial Office, (2020). *Overview of Chiang Mai Province. Strategy and Information for Provincial Development Group*, Chiang Mai Provincial Office. [Online]. Available: https://www.chiangmai.go.th/managing/public/D8/8D12Nov2020103220.pdf. [Accessed: May 21, 2025].

[32] Woźniak, E. and Aleksandrowicz, S., (2019). Self-Adjusting Thresholding for Burnt Area Detection Based on Optical Images. *Remote Sensing*, Vol. 11(22). https://doi.org/10.3390/rs11222669.

[33] Sukmono, A., Hadi, F., Widayanti, E., Nugraha, A. L. and Bashit, N., (2023). Identifying Burnt Areas in Forests and Land Fire Using Multitemporal Normalized Burn Ratio (NBR) Index on Sentinel-2 Satellite Imagery. *International Journal of Safety and Security Engineering*, Vol. 13(3). https://doi.org/10.18280/ijsse.130309.

[34] Congalton, R. G., (1991). A Review of Assessing the Accuracy of Classifications of Remotely Sensed Data. *Remote Sensing of Environment*, Vol. 37(1). https://doi.org/10.1016/0034-4257(91)90048-B.

[35] Anderson, J. R., Hardy, E. E., Roach, J. T. and Witmer, R. E., (1976). *A Land Use and Land Cover Classification System for Use with Remote Sensor Data*. U.S. Geological Survey Professional Paper 964. U.S. Government Printing Office, Washington, D.C. [Online]. Available: https://pubs.usgs.gov/pp/0964/report.pdf. [Accessed: May 21, 2025].

[36] Landis, J. R. and Koch, G. G., (1977). The Measurement of Observer Agreement for Categorical Data. *Biometrics*, Vol. 33(1). https://doi.org/10.2307/2529310.

[37] Zec, S., Soriani, N., Comoretto, R. and Baldi, I., (2017). High Agreement and High Prevalence: The Paradox of Cohen's Kappa. *The Open Nursing Journal*, Vol. 11. https://doi.org/10.2174/1874434601711010211.

[38] Pontius, R. G. Jr. and Millones, M., (2011). Death to Kappa: Birth of Quantity Disagreement and Allocation Disagreement for Accuracy Assessment. *International Journal of Remote Sensing*, Vol. 32(15). https://doi.org/10.1080/01431161.2011.552923.

[39] Congalton, R. G. and Green, K., (2019). *Assessing the Accuracy of Remotely Sensed Data: Principles and Practices*. 3rd ed. CRC Press. [Online]. Available: https://doi.org/10.1201/9780429052729. [Accessed: Dec. 1, 2025].

[40] Han, A., Qing, S., Bao, Y., Na, L., Bao, Y., Liu, X., Zhang, J. and Wang, W., (2021). Short-Term Effects of Fire Severity on Vegetation Based on Sentinel-2 Satellite Data. *Sustainability*, Vol. 13(1). https://doi.org/10.3390/su13010432.

[41] Khamrueangwong, T. and Kamthonkiat, D., (2021). Burn Indices from Landsat 8: Restrictions on Its Application. *Burapha Science Journal*, Vol. 26(2); 1308-1325. [Online]. Available: https://li05.tci-thaijo.org/index.php/buuscij/article/view/1433/858. [Accessed: May 21, 2025].

[42] Pleniou, M. and Koutsias, N., (2013). Sensitivity of Spectral Reflectance Values to Different Burn and Vegetation Ratios: A Multi-Scale Approach Applied in a Fire Affected Area. *ISPRS Journal of Photogrammetry and Remote Sensing*, Vol. 79. https://doi.org/10.1016/j.isprsjprs.2013.02.016.

[43] Ngadze, F., Mpakairi, K. S., Kavhu, B., Ndaimani, H. and Maremba, M. S., (2020). Exploring the Utility of Sentinel-2 MSI and Landsat 8 OLI in Burned Area Mapping for a Heterogenous Savannah Landscape. *PLOS ONE*, Vol. 15(5). https://doi.org/10.1371/journal.pone.0232962.

[44] van Dijk, D., Shoaie, S., van Leeuwen, T. and Veraverbeke, S., (2021). Spectral Signature Analysis of False Positive Burned Area Detection from Agricultural Harvests using Sentinel-2 data. *International Journal of Applied Earth Observation and Geoinformation*, Vol. 97. https://doi.org/10.1016/j.jag.2021.102296.

[45] Wooster, M. J., Roberts, G. J., Giglio, L., Roy, D. P., Freeborn, P. H., Boschetti, L., Justice, C., Ichoku, C., Schroeder, W., Davies, D., Smith, A. M. S., Setzer, A., Csiszar, I., Strydom, T., Frost, P., Zhang, T., Xu, W., de Jong, M. C., Johnston, J. M., Ellison, L., Vadrevu, K., Sparks, A. M., Nguyen, H., McCarty, J., Tanpipat, V., Schmidt, C. and San-Miguel-Ayanz, J., (2021). Satellite Remote Sensing of Active Fires: History and Current Status, Applications and Future Requirements. *Remote Sensing of Environment*, Vol. 267. https://doi.org/10.1016/j.rse.2021.112694.

[46] Hu, X., Ban, Y. and Nascetti, A., (2021). Sentinel-2 MSI Data for Active Fire Detection in Major Fire-Prone Biomes: A Multi-Criteria Approach. *International Journal of Applied Earth Observation and Geoinformation*, Vol. 101. https://doi.org/10.1016/j.jag.2021.102347

[47] Liu, S., Zheng, Y., Dalponte, M. and Tong, X., (2020). A Novel Fire Index-Based Burned Area Change Detection Approach using Landsat-8 OLI Data. *European Journal of Remote Sensing*, Vol. 53(1). https://doi.org/10.1080/22797254.2020.1738900.

[48] Pacheco, A. d. P., da Silva Junior, J. A., Ruiz-Armenteros, A. M., Henriques, R. F. F. and de Oliveira Santos, I., (2023). Analysis of Spectral Separability for Detecting Burned Areas Using Landsat-8 OLI/TIRS Images under Different Biomes in Brazil and Portugal. *Forests*, Vol. 14(4). https://doi.org/10.3390/f14040663.

[49] Zhang, Z., Qi, B., Huang, S., Long, T., He, G., Wang, G. and Sun, Y., (2025). Burned Area Detection and Estimation of Fire Carbon Emissions in Canada in 2023 using Landsat 8/9 and Sentinel 2 Data. *Remote Sensing Letters*, Vol. 16(8). https://doi.org/10.1080/2150704X.2025.2513558.

[50] Smiraglia, D., Filipponi, F., Mandrone, S., Tornato, A. and Taramelli, A., (2020). Agreement Index for Burned Area Mapping: Integration of Multiple Spectral Indices Using Sentinel-2 Satellite Images. *Remote Sensing*, Vol. 12(11). https://doi.org/10.3390/rs12111862.

[51] Tiengo, R., Merino-De-Miguel, S., Uchôa, J., Guiomar, N. and Gil, A., (2025). Burned Areas Mapping Using Sentinel-2 Data and a Rao's Q Index-Based Change Detection Approach: A Case Study in Three Mediterranean Islands' Wildfires (2019–2022). *Remote Sensing*, Vol. 17(5). https://doi.org/10.3390/rs17050830.